Evidence of neocortex-like primitive laminar pallium in avian embryo and its organization by microRNA-19b

Archita Mishra, Niveda Udaykumar[1], Suvimal Kumar Sindhu[2]*, Jonaki Sen*

Indian Institute of Technology Kanpur, Kanpur-208016, UP, India

[1]St. Jude Children's Hospital, Memphis, TN, 38105, USA

[2]Yale School of Medicine, New Haven, CT, 06511, USA

***Email:** suvimal.sindhu@yale.edu**;** jonaki.sen@iitk.ac.in

Author Contributions:

S.K.S., and J.S. designed study; S.K.S., A.M., N.U. performed experiments; S.K.S., A.M., N.U., and J.S. analyzed data; J.S. Supervised; S.K.S., A.M., and J.S. wrote the paper.

Competing Interest Statement: No competing interest.

Classification: Major: Biological Sciences; **Minor:** Neuroscience

Keywords: miR-19b, Fezf2, Pallium, Chick, Mef2c, Neocortex

This file includes:

Main Text
Figures 1 to 2

Abstract

Unlike the mammalian neocortex, where neurons are highly organized in six-layers, the avian pallium contains spatially segregated clusters of neurons. Although the quest to find similarities between the avian pallium and the mammalian neocortex has long been pursued, the extent of similarity between the two in terms of pallial organization is not completely explored. This study reveals the existence of a transient two-layer structure of the developing chick pallium, mirroring the order of neocortical layers as well as the proliferation-dependent mode of specification that is partly regulated by microRNA-19b. This suggests a closer ontogenetic similarity between the avian pallium and the mammalian neocortex, reinforcing the idea of convergent evolution of cortical lamina from common amniote ancestry.

Main Text

Introduction

The study of how a laminar pallium such as the mammalian neocortex evolved from the nonlaminar pallium of birds and reptiles is a long-standing interest in the field of neuroscience (1, 2). The mammalian neocortex features a six-layered laminar pallium, with neocortical neurons following an inside-out birth and migration pattern (3). Unlike mammals, the avian pallial neurons follow an outside-in birth pattern, with first-born neurons atop and subsequent neurons migrating beneath, which are specified as spatially segregated nuclei instead of laminae (4). However, birds do exhibit region-specific laminar organization in the primary auditory cortex (5) and the hyperpallium region (6). Moreover, examination of expression of homologous neocortical layer markers and, projections of developing avian pallial nuclei has revealed the presence of neocortex-like neuronal subtypes in birds (1, 7, 8). Nevertheless, the initial steps and mechanisms of formation of such homologous neurons in the avian brain are not well-studied. In this study, we investigated the expression pattern of the deep-layer neocortical marker (Fezf2) and the upper-layer marker (Mef2c) (2) at early stages of avian pallial development and explored the mode of production of these neurons to elucidate similarities in organization between the avian pallium and the mammalian neocortex.

Results & Discussion

To comprehensively analyze expression pattern of Fezf2 and Mef2c in the avian pallium, we analyzed it at Hamilton-Hamburger stage 28 (HH28) (9) or embryonic day 5.5 (E5.5) and at HH32 (E7.5) and found that at HH28, Fezf2 was expressed in the ventricular zone (VZ) of the dorsomedial region and the subventricular zone (SVZ) of the dorsal pallium (Fig. 1A). Upon performing immunostaining with Neurod1, we ascertained the identity of Fezf2+ cells in the SVZ as postmitotic immature neurons as they were found to co-express Neurod1 (Fig.1A, Inset). On the other hand, Mef2c expression was found in the cells atop the Fezf2+ cells in the SVZ (Fig. 1A). Thus, the expression of Fezf2 and Mef2c reveal a bi-layered structure at HH28, mirroring the order of neocortical lamina (2). However, at advanced stages i.e. HH32 (Fig. 1B), HH36 (E10) and at post-natal day 0 (P0), expression domains of these two markers became spatially segregated, with Fezf2 in the hyperpallium and parahippocampal area (APH) and Mef2c in the

mesopallium (Msp) (1, 8). Therefore, with the progress of development in the avian pallium, the Fezf2+ and Mef2c+ neurons become spatially segregated as opposed to the earlier stage when they are in a bi-layered structure. The presence of such transient lamina at early stages in the avian pallium suggests that the common ancestors of birds and mammals may have had primitive pallial lamina such as this.

Taking cues from studies performed in mice where deep-layer neurons are born due to early cessation of neurogenesis (10, 11), we analyzed the dynamics of cell proliferation in the developing chick pallium in order to understand the mechanism of appearance of Fezf2 expression in the deep-layer at HH28. Immunostaining with PH3 revealed that at HH25 (E4.5) there was homogenous proliferation across the dorsal pallium, however at HH30 (E6.5) proliferation ceases in the dorsomedial region, while the cells in the lateral region, dorsal ventricular ridge (DVR) continued to proliferate, which finally ceases at HH35 (E8.5) (Fig. 1C) as observed in previous studies (7, 8). Moreover, Neurod1 expression was negligible at HH25, however, at the HH30 it was predominant in the SVZ of the presumptive Wulst area. Subsequently, at HH35 Neurod1 expression was restricted to the SVZ of DVR area alone, with some additional expression in the Hippocampal and APH region (Fig.1C), (7). Taken together, these data indicate that NPCs in the dorso-medial region cease proliferation earlier than the dorso-lateral region. Hence it is postulated that early cessation of proliferation of NPCs may lead to production of Fezf2+ neurons. To determine the role of cell proliferation in the production of deep-layer neurons, we overexpressed CDKN1A, a cell-cycle inhibitor (12) in the chick forebrain at an early stage. We observed that this induced ectopic expression of Fezf2+; Neurod1+ neurons (Fig. 1D), indicating that inhibition of the cell-cycle is sufficient for generation of Fezf2+; Neurod1+ neurons in the developing chick pallium (Fig. 1D). Interestingly, NPCs in the developing chick pallium exhibit a spatially-biased potential for generation of Fezf2+ and Mef2c+ neurons. This is in contrast to an *in vitro* study wherein chicken NPCs were shown to generate both deep-layer and upper-layer neurons, similar to that in mammals (8, 11).

To identify candidate cell-cycle regulators in this context, based on literature search, we selected a microRNA, miR-19b, known to regulate cell proliferation in the mouse forebrain (13) and also is expressed in the VZ of the chick pallium at HH25 (14). Our analysis revealed that the expression domain of miR-19b in the VZ at HH30 is mutually exclusive from that of Neurod1 which is expressed in the SVZ (Fig.1E). In order to determine the mechanism of cell-cycle regulation by miR-19b, we proceeded to identify *in silico* predicted target mRNAs using the miR database (miRDB) (15) and Targetscan (16) and 423 potential targets were selected from the intersection of these (Fig. 1F, Table S1-3). Gene ontology analysis revealed that several targets of miR-19b were related to cellular senescence (Fig. 1F, G). For further investigation, we selected two predicted targets of miR-19b that were well-known inhibitors of the cell-cycle i.e. E2f8 and Neurod1 based on their robust expression in the developing chick forebrain (7, 17).

Analysis of target regions of E2f8 and Neurod1 across different species using TargetScan (16) revealed evolutionary conserved target regions. We then tested if miR-19b can regulate these transcripts through their respective target regions (See materials & methods). For this, we performed a sensor assay (14), by expressing fused transcripts of target regions of E2f8 and Neurod1 with a mCherry reporter coding sequence (CDS) co-expressed with miR-19b and control constructs (Fig. 1H, I). This led to

downregulation of mCherry expression in the presence of miR-19b in comparison to the control, indicating that miR-19b can regulate these transcripts using their target regions.

We performed gain-of-function (GoF) and loss-of-function (LoF) experiments with miR-19b using constructs expressing miR-19b and Sponge-19b, respectively (See materials and methods), to determine if E2f8 and Neurod1 mRNAs are targets of miR-19b *in vivo* in the developing chick pallium (14). Indeed miR-19b was found to be sufficient to regulate the expression of E2f8 (Fig. 2A) as well as Neurod1 (Fig. 2C). However, while loss of miR-19b expression indicated that it is necessary for E2f8 expression (Fig. 2B), the same was not true for Neurod1 (Fig. 2D). We hypothesize that the lack of ectopic expression of Neurod1 upon LoF of miR-19b indicates the presence of other factors inhibiting Neurod1 expression in this region.

To establish the role of miR-19b in regulation of cell proliferation, we used flow cytometry to measure DNA quantity in chicken fibroblast cells (DF1) transfected with miR-19b. We observed that, compared to the control, miR-19b expression led to an increase in cells in the S-phase and M-phase at the expense of cells in G0/G1 (Fig. 2E, F). We investigated the ability of miR-19b to regulate cell proliferation in the developing chick pallium using EdU labeling. For this, we expressed miR-19b, Sponge-19b and control constructs in chick embryo forebrain at E3.5 (HH23) and EdU was added 2 hours before harvesting at E4.5 (HH25). The quantification of percentage of GFP+ cells that are also Edu+ revealed that indeed miR-19b promotes incorporation of EdU whereas Sponge-19b significantly reduced EdU-labelling in comparison to control (Fig. 2G). In addition, when we performed GoF and LoF experiments with miR-19b at E8, we found that indeed miR-19b overexpression led to an increase in percentage of GFP+ cells that are also PH3+ whereas deficiency of miR-19b led to a reduction of the same, in comparison to the control (Fig. 2H). Taken together, these data suggest that miR-19b plays a significant role in regulation of cell proliferation in the developing chick pallium.

Our observation of cell cycle inhibition leading to ectopic Fezf2 expression (Fig. 1D) taken together with the establishment of miR-19b as a regulator of cell proliferation, prompted us to test if miR-19b may regulate the expression of deep-layer neuronal markers. For this, we carried out LOF of miR-19b by overexpressing Sponge-19b in the VZ and found that indeed removal of miR-19b leads to ectopic expression of Fezf2+ in these cells (Fig. 2I). This mechanism of proliferation-dependent specification of pallial neurons is similar to that observed during neuronal specification in the mammalian neocortex (10), indicating conservation in mechanism(s) of cortical neuronal specification between aves and mammals.

One characteristic feature of deep-layer neocortical neurons is the formation of sub-cerebral/extra-telencephalic long-range projections to establish the cortico-spinal tract. Fezf2 is critical for specification of deep-layer neurons and their emerging projections in mammals (18). In the avian system, Fezf2 expression is observed transiently at an early stage of pallial development, hence it is impossible to study conservation in projections for these neurons as projections emerge from relatively more mature neurons. However, at later stages of development, Fezf2 is found to be expressed robustly in the rostral hyperpallium region of the somatosensory wulst (1) and interestingly, neurons from this region, show similar long-range projection to the red nucleus apart from other nuclei, which further project to the spinal cord (19). This lends support to the idea that Fezf2 orchestrates a similar function in the avian pallium as in the mammalian brain by

generating long-range projection although at a later stage of development. Moreover, the presence of Fezf2+ neurons in the deep-layer in the early chick embryo points to a correlation between deep-layer and long-range projection albeit at a different stage as compared to mammals.

On the other hand, the dorsal DVR region of the avian pallium exhibits prolonged cell proliferation and expression of Mef2c an upper layer marker in the lateral DVR i.e. mesopallium, indicating a correlation between prolonged proliferation of NPCs and upper-layer neuron formation, similar to the mammalian neocortex (8). However, at earlier stages in the avain pallium, where NPCs are still early in terms of proliferation, there is a transient bi-layer structure expressing Fezf2 and Mef2c. This may be explained by one of the two following mechanisms: a) conversion of Fezf2+ neurons to Mef2c+ neurons by achieving knock-down of Fezf2 expression, (supported by the fact that Fezf2 LoF lead to conversion of DL neurons into UL neurons in the mouse (18)) and b) migration of relatively earlier born NPCs, rather than the NPCs that generate Fezf2+ neurons, past the Fezf2+ neurons to sit above them. The second phenomenon is less likely to happen as avian species mainly exhibit outside-in pattern of migration (4).

In conclusion, we have shown that pallium of birds does have a transient laminar state akin to that of the mammalian neocortex in terms of organization and cell-cycle dependent mode of production of neurons. This argues in favor of birds and mammals having common ancestry with a similar mode of laminar pallium formation.

Materials and Methods

The chicken eggs form white leg horn hen were obtained from Kanpur, India.
Experimental details are provided in Supplementary Information.

Data Availability

All data included in the manuscript.

Acknowledgments

We acknowledge Prof. Amitabha Bandhopadhyay (IIT Kanpur, India) for valuable suggestions on the manuscript. We are grateful to Neetu Dey (IIT Kanpur) for confocal microscopy, and D. N. Vishwakarma (CDRI, Lucknow) for flow cytometry. This work was funded by SERB, Department of Science & Technology, Govt. of India. (EMR/2016/000886) to J.S. CSIR, Govt. of India supported S.K.S. for his Ph.D. (09/092(0824)/2011-EMR-I). A.M. and N.U. were supported by MHRD, Govt. of India.

References

1. J. Dugas-Ford, J. J. Rowell, C. W. Ragsdale, Cell-type homologies and the origins of the neocortex. *Proc Natl Acad Sci U S A* **109**, 16974-16979 (2012).
2. B. J. Molyneaux, P. Arlotta, J. R. Menezes, J. D. Macklis, Neuronal subtype specification in the cerebral cortex. *Nat Rev Neurosci* **8**, 427-437 (2007).

3. J. B. Angevine, Jr., R. L. Sidman, Autoradiographic study of cell migration during histogenesis of cerebral cortex in the mouse. *Nature* **192**, 766-768 (1961).
4. H. M. Tsai, B. B. Garber, L. M. Larramendi, 3H-thymidine autoradiographic analysis of telencephalic histogenesis in the chick embryo: I. Neuronal birthdates of telencephalic compartments in situ. *J Comp Neurol* **198**, 275-292 (1981).
5. Y. Wang, A. Brzozowska-Prechtl, H. J. Karten, Laminar and columnar auditory cortex in avian brain. *Proc Natl Acad Sci U S A* **107**, 12676-12681 (2010).
6. M. Stacho *et al.*, A cortex-like canonical circuit in the avian forebrain. *Science* **369** (2020).
7. S. Gupta, R. Maurya, M. Saxena, J. Sen, Defining structural homology between the mammalian and avian hippocampus through conserved gene expression patterns observed in the chick embryo. *Dev Biol* **366**, 125-141 (2012).
8. I. K. Suzuki, T. Kawasaki, T. Gojobori, T. Hirata, The temporal sequence of the mammalian neocortical neurogenetic program drives mediolateral pattern in the chick pallium. *Dev Cell* **22**, 863-870 (2012).
9. V. Hamburger, H. L. Hamilton, A series of normal stages in the development of the chick embryo. 1951. *Dev Dyn* **195**, 231-272 (1992).
10. S. K. McConnell, C. E. Kaznowski, Cell cycle dependence of laminar determination in developing neocortex. *Science* **254**, 282-285 (1991).
11. Q. Shen *et al.*, The timing of cortical neurogenesis is encoded within lineages of individual progenitor cells. *Nat Neurosci* **9**, 743-751 (2006).
12. C. Deng, P. Zhang, J. W. Harper, S. J. Elledge, P. Leder, Mice lacking p21CIP1/WAF1 undergo normal development, but are defective in G1 checkpoint control. *Cell* **82**, 675-684 (1995).
13. S. Bian *et al.*, MicroRNA cluster miR-17-92 regulates neural stem cell expansion and transition to intermediate progenitors in the developing mouse neocortex. *Cell Rep* **3**, 1398-1406 (2013).
14. S. K. Sindhu, N. Udaykumar, M. A. A. Zaidi, A. Soni, J. Sen, MicroRNA-19b restricts Wnt7b to the hem, which induces aspects of hippocampus development in the avian forebrain. *Development* **146** (2019).
15. Y. Chen, X. Wang, miRDB: an online database for prediction of functional microRNA targets. *Nucleic Acids Res* **48**, D127-D131 (2020).
16. V. Agarwal, G. W. Bell, J. W. Nam, D. P. Bartel, Predicting effective microRNA target sites in mammalian mRNAs. *Elife* **4** (2015).
17. J. Christensen *et al.*, Characterization of E2F8, a novel E2F-like cell-cycle regulated repressor of E2F-activated transcription. *Nucleic Acids Res* **33**, 5458-5470 (2005).
18. B. Chen *et al.*, The Fezf2-Ctip2 genetic pathway regulates the fate choice of subcortical projection neurons in the developing cerebral cortex. *Proc Natl Acad Sci U S A* **105**, 11382-11387 (2008).
19. L. Medina, A. Reiner, Do birds possess homologues of mammalian primary visual, somatosensory and motor cortices? *Trends Neurosci* **23**, 1-12 (2000).

Figure Legend(s):

Figure 1. A transient, laminar structure in the embryonic chick pallium and miR-19b mediated regulation of E2f8 and Neurod1 in vitro. (A) & (B) Expression pattern of Fezf2 and Mef2c at E5.5 and E7.5 in chicken forebrain. 1(A) Inset shows cells double-positive for Fezf2 and Neurod1 in the SVZ. N=3, Scale bar: 300µm, 25µm (A-Inset), 150µm (B-inset). Intensity plot for Fezf2 and Mef2c. (C) Immunostaining for PH3 and Neurod1 with intensity plot. Circles show a magnified view. N=3, Scale bar: 500µm, 125µm (inset) (D) Images showing the effect of overexpressing CDKN1A on Fezf2 and Neurod1 expression. Circles showing magnified view. Bar graph showing quantification. N=4, Scale bar: 300µm. (E) Neurod1 expression at SVZ and miR-19b at VZ. Insets show magnified images. N=3, Scale bar: 100µm, 30µm (inset) (F) Venn diagram displaying miRNA targets predicted by miRDB and TargetScan. Gene ontology analysis for common targets. (G) List of functionally validated targets. Red square adjacent to a gene indicates its previously reported role in process/pathway mentioned on the top row. (H) & (I) Sensor assay to show target region of E2f8 and Neurod1 regulated by miR-19b. mCherry intensity was quantified and plotted. Scale bar: 100µm, Plot bar represent mean ± s.e.m., N=3 wells, t-test was performed, **p≤0.01 and ****p≤0.0001. A.U.= arbitrary unit. DM= dorso-medial, V= ventricle, DP= dorsal pallium, VP= ventral pallium, VZ= ventricular zone, SVZ= sub-ventricular zone, DL= deep layer, UL= upper layer, APH= parahippocampal area, HA= hyperpallium apicale, Msp= mesopallium, Ndp= nidopallium, Str= striatum, DVR= dorsal ventricular ridge.

Figure 2. miR-19b regulates E2f8 and Neurod1 in vivo and controls proliferation and Fezf2 expression. Effect of miR-19b manipulation on E2f8 (A) & (B) and on Neurod1 expression (C) & (D). N=4, Scale bar: 300µm (A, B), 50µm (C, D), 25µm (C-inset, D-inset), Bar graph represents mean. (E) Schema for flow cytometry experiment. (F) Cell cycle distribution of DF1 cells transfected with control and miR-19b expressing constructs. (G) & (H) Cell proliferation analysis by EdU-labeling & PH3 upon miR-19b manipulation. White/Yellow arrowheads indicate double-positive cells. N=3, Scale bar: 200µm (G), 50µm (H), 300µm (I). (I) Effect of miR-19b inhibition on Fezf2 expression. Bar graph plotted for quantification. N=4, Plot bar represents mean ± S.E.M. A.U.= arbitrary unit. ns= not significant; VZ= ventricular zone, SVZ= sub-ventricular zone. t-test was performed, *p≤0.1, **p≤0.01 and ***p≤0.001, ns = non-significant.

Figure 1

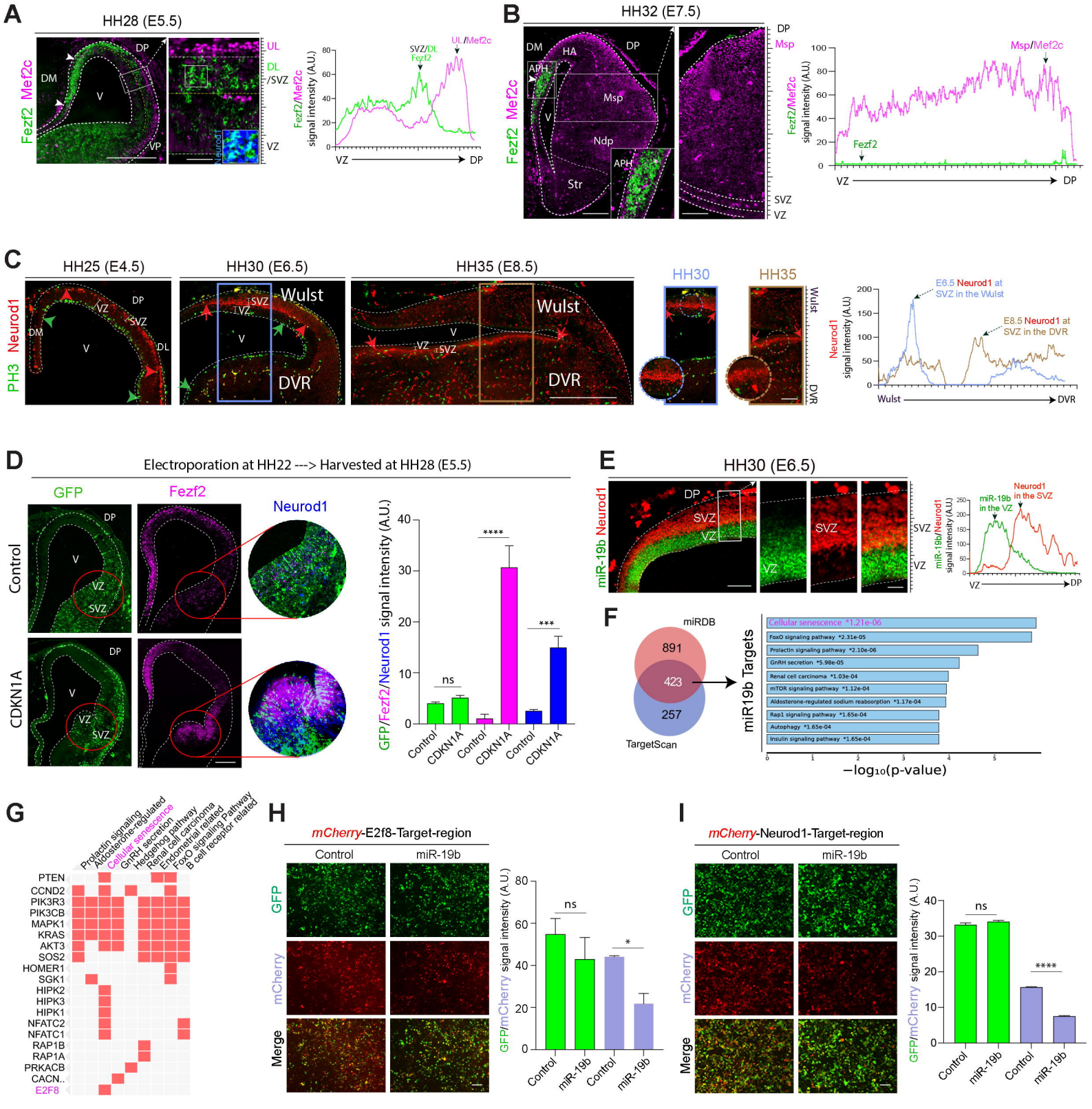
A
HH28 (E5.5)
Fezf2 Mef2c
DM
V
DP
VP
UL
DL
/SVZ
VZ
Neurod1
Fezf2/Mef2c signal intensity (A.U.)
SVZ/DL Fezf2
UL/Mef2c
VZ
DP
B
HH32 (E7.5)
DM
HA
DP
APH
Msp
V
Ndp
Str
Msp/Mef2c
Fezf2
C
HH25 (E4.5)
HH30 (E6.5)
HH35 (E8.5)
PH3 Neurod1
VZ
SVZ
DP
DM
V
DL
Wulst
DVR
HH30
HH35
Neurod1 signal intensity (A.U.)
E6.5 Neurod1 at SVZ in the Wulst
E8.5 Neurod1 at SVZ in the DVR
D
Electroporation at HH22 ---> Harvested at HH28 (E5.5)
GFP
Fezf2
Neurod1
Control
CDKN1A
GFP/Fezf2/Neurod1 signal intensity (A.U.)
ns
****
***
E
HH30 (E6.5)
miR-19b Neurod1
DP
SVZ
VZ
miR-19b/Neurod1 signal intensity (A.U.)
miR-19b in the VZ
Neurod1 in the SVZ
F
miRDB
891
423
257
TargetScan
miR19b Targets
Cellular senescence *1.21e-06
FoxO signaling pathway *2.31e-05
Prolactin signaling pathway *2.10e-06
GnRH secretion *5.98e-05
Renal cell carcinoma *1.03e-04
mTOR signaling pathway *1.12e-04
Aldosterone-regulated sodium reabsorption *1.17e-04
Rap1 signaling pathway *1.65e-04
Autophagy *1.65e-04
Insulin signaling pathway *1.65e-04
−log10(p-value)
G
Prolactin signaling
Aldosterone-regulated
Cellular senescence
GnRH secretion
Hedgehog pathway
Renal cell carcinoma
Endometrial related
FoxO signaling Pathway
B cell receptor related
PTEN
CCND2
PIK3R3
PIK3CB
MAPK1
KRAS
AKT3
SOS2
HOMER1
SGK1
HIPK2
HIPK3
HIPK1
NFATC2
NFATC1
RAP1B
RAP1A
PRKACB
CACN..
E2F8
H
mCherry-E2f8-Target-region
Control
miR-19b
GFP
mCherry
Merge
GFP/mCherry signal intensity (A.U.)
ns
*
I
mCherry-Neurod1-Target-region
Control
miR-19b
GFP
mCherry
Merge
GFP/mCherry signal intensity (A.U.)
ns
****

Figure 2

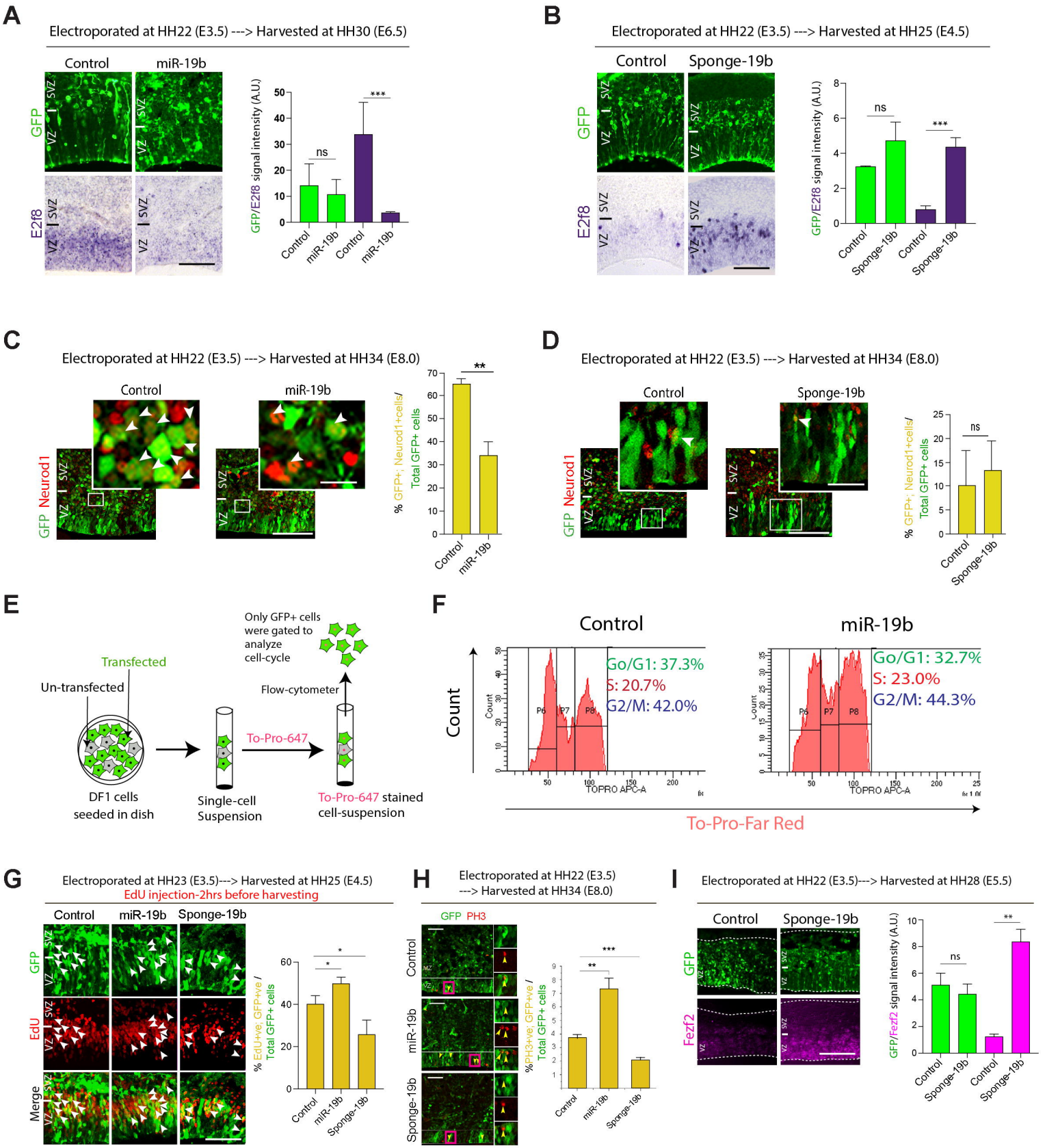
A
Electroporated at HH22 (E3.5) ---> Harvested at HH30 (E6.5)
Control
miR-19b
GFP
E2f8
VZ
SVZ
GFP/E2f8 signal intensity (A.U.)
ns
***
Control
miR-19b
Control
miR-19b
B
Electroporated at HH22 (E3.5) ---> Harvested at HH25 (E4.5)
Control
Sponge-19b
GFP
E2f8
GFP/E2f8 signal intensity (A.U.)
ns
***
Control
Sponge-19b
Control
Sponge-19b
C
Electroporated at HH22 (E3.5) ---> Harvested at HH34 (E8.0)
Control
miR-19b
GFP Neurod1
% GFP+; Neurod1+cells/ Total GFP+ cells
**
Control
miR-19b
D
Electroporated at HH22 (E3.5) ---> Harvested at HH34 (E8.0)
Control
Sponge-19b
GFP Neurod1
% GFP+; Neurod1+cells/ Total GFP+ cells
ns
Control
Sponge-19b
E
Only GFP+ cells were gated to analyze cell-cycle
Transfected
Un-transfected
Flow-cytometer
To-Pro-647
DF1 cells seeded in dish
Single-cell Suspension
To-Pro-647 stained cell-suspension
F
Control
miR-19b
Count
Go/G1: 37.3%
S: 20.7%
G2/M: 42.0%
Go/G1: 32.7%
S: 23.0%
G2/M: 44.3%
P6
P7
P8
TOPRO APC-A
To-Pro-Far Red
G
Electroporated at HH23 (E3.5)---> Harvested at HH25 (E4.5)
EdU injection-2hrs before harvesting
Control
miR-19b
Sponge-19b
GFP
EdU
Merge
% EdU+ve; GFP+ve / Total GFP+ cells
*
*
Control
miR-19b
Sponge-19b
H
Electroporated at HH22 (E3.5) ---> Harvested at HH34 (E8.0)
GFP PH3
Control
miR-19b
Sponge-19b
%PH3+ve; GFP+ve / Total GFP+ cells
***
**
Control
miR-19b
Sponge-19b
I
Electroporated at HH22 (E3.5)---> Harvested at HH28 (E5.5)
Control
Sponge-19b
GFP
Fezf2
GFP/Fezf2 signal intensity (A.U.)
ns
**
Control
Sponge-19b
Control
Sponge-19b